Journal of Physics: Conference Series

PAPER • **OPEN ACCESS**

Effect of body motion on the wave loads computed with CFD on the INO-WINDMOOR floater

Effect of body motion on the wave loads computed with CFD on the INO-WINDMOOR floater

A Califano[1], **P A Berthelsen**[1] **and N M Magalhaes Duque Da Fonseca**[1]

[1] SINTEF Ocean, Trondheim NO-7465 NORWAY

andrea.califano@sintef.no

Abstract. CFD simulations were carried out on the 1:40 model of the INO WINDMOOR floater in regular waves to extract hydrodynamic loads, both on the structure, the single columns and sections from each column. Three different approaches for the platform motion were used, (i) fixed, i.e., restrained from motion, (ii) prescribed, i.e., forcing the floater to follow the motion recorded during model tests and (iii) 6 DOF, i.e., allowing the floater to move according to external forces from waves and anchor lines. The obtained results show the effect of the free surface on the local drag forces at sections with different submergences, which are important to include when modelling the motion with simplified methods based on pre-computed force coefficients. A comparison of the surge force shows that the amplitudes of the loads obtained with moving platform are reduced compared to the corresponding fixed case. The mean total surge force computed on the single columns and the whole platform show small quantitative differences between the different methods. The motion responses of the platform for surge and heave obtained with CFD are in fair agreement with the experiments.

1. Introduction

The last decades have shown an increased demand for renewable energy requiring greater power and minimal intervention on the landscape. This global trend has been a driver of the technology development needed to install and operate large floating structures located offshore, hosting wind turbines.

Floating wind turbines (FWT) located in deep and shallow water far from the coastline are moored to the sea bottom, and their design rely on accurate predictions of mean and slowly varying forces and motions. State of the art numerical models based on linear potential theory are known to underestimate the mean and slowly varying (low frequency) motions, especially in large and steep waves. For slender structures like semi-submersibles and spars, this underestimation is believed to be largely due to higher order viscous effects and wave-current interaction effects. Viscous effects are usually applied as a sea state dependent correction to the drift force coefficients from potential theory.

Wave exciting loads on column stabilized large-volume structures can be decomposed into a drag component related to flow separation and a potential flow component. Linear or second order potential flow theory are usually applied to formulate the equations of motion, where these force components are calculated for the restrained body. The drag force component representative of the restrained body case can also be applied within a "relative velocity approach", where the incident wave kinematics are combined with the body motions to define the relevant velocity.

The underestimation of the input drag coefficients computed on a restrained structure might result in an inaccurate estimation of design structural loads, reducing the expected life of the structures.

As part of ongoing research aiming at improving modelling of viscous forces on offshore floating structures, CFD simulations were carried out on the 1:40 model of the INO WINDMOOR floater [1] in regular waves to extract hydrodynamic loads, both on the structure, the single columns and sections from each column.

This geometry has been thoroughly tested in the ocean basin facilities of SINTEF Ocean [2], and its performance in waves studied to extract Morison force coefficients [3] and by means of CFD simulations [4]. Extensive literature exists on the application of computational fluid dynamics simulations to offshore structures. CFD has also been widely applied to predict the response of a moored floating wind platform to wave excitation [5] [6].

2. Model

The INO WINDMOOR structure [1] has a triangular shape composed by three vertical columns joined at the bottom by pontoons and at the top by deck beams (Figure 1). While waves are in the positive x-axis direction, there will be two columns upstream on the port and starboard side, symmetrical with respect to the centreline plane. The third column downstream in the middle of the centreline plane is supporting the wind turbine tower. All analyses were carried out at a model scale of 1:40. Full-scale dimensions and mass properties of the INO WINDMOOR structure are given in Table 1 and Table 2, respectively. The structure has a draft T of 15.5 m and the water depth is 150 m.

Each column is split into 23 sections with equal height of 1 m, where local loads are computed. These sections are numbered as z_j, where j is the vertical distance of the centre position from the water line, such as z_0 corresponds to the section piercing the water line (Figure 1).

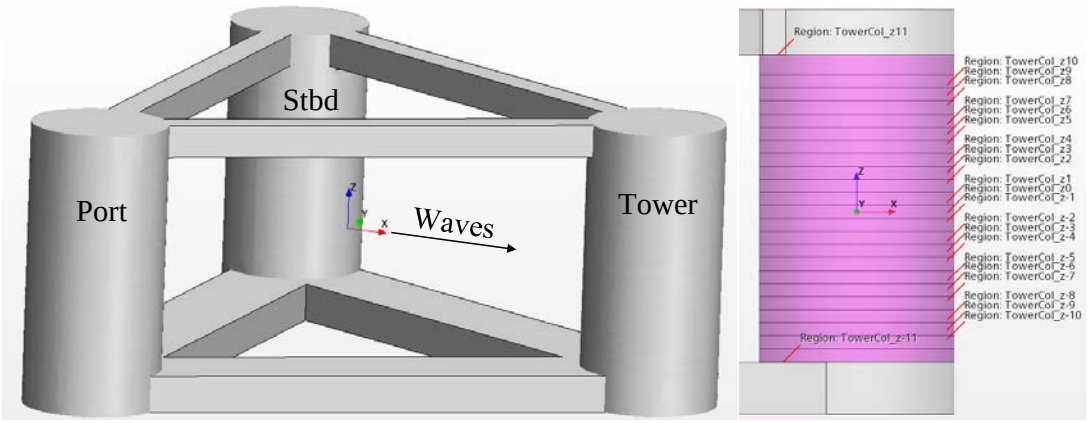

Figure 1. Platform model (left) and division in sections of the tower column (right).

Table 1. Main dimensions of the INO WINDMOOR structure (full-scale).

Parameter	Value [m]
Platform Height	31
Column diameter	15
Column C-C distance	61
Pontoon Width	10
Pontoon Height	4
Deck beams Width	3.5
Deck beams Height	3.5

Table 2. Mass properties of the INO WINDMOOR structure (full-scale).

	Parameter	Value	Unit
	Mass	14 124	t
Radius	R_{xx}	43.62	m
of	R_{yy}	44.01	m
gyration	R_{zz}	29.87	m
Centre	x	0	m
of	y	0	m
gravity	z	3.94	m

2.1. Numerical set up

The inner computational domain is centred at the platform centre and has dimensions of 4 and 3 times the column's center-to-center distance in the length and width direction, respectively. This inner domain is extended by 1, 1.5 and 0.5 wave lengths at the inlet, outlet and side boundaries, respectively.

The solution of the input wave is forced at the lateral boundaries and is gradually blended with the computed numerical solution until the inner numerical domain. The forcing function has a $\cos^2$-variation with maximum value of 5. This method is often referred to as Euler Overlay Method (EOM), as it blends the outer Euler zone with the inner CFD domain through an overlay zone [7]. A top view of the forcing coefficient is depicted in Figure 2.

A velocity inlet boundary condition was imposed at the inlet and outlet boundaries, perpendicular to the wave and current direction. An outlet condition is imposed on the top, whereas the side boundaries are modelled as symmetry planes. A no-slip wall condition is imposed on the structure, whereas a slip condition is used on the bottom.

Simulations are run with the software Simcenter STAR-CCM+ 2020.3 Build 15.06.007 [8].

The interface between air and water is captured with a volume of fluid (VOF) model using a high-resolution interface capturing (HRIC) convection scheme. Turbulence is solved with an improved delayed detached eddy simulation (IDDES), resolving the large scales of turbulence and modelling small-scale motions. A low-Reynolds number approach is used for the near-wall treatment, requiring a fine near-wall mesh height.

An implicit unsteady solver with second order temporal discretization is used to solve the transient problem, with constant time-step as 1/500 the wave period.

2.1.1. Waves. Waves are modelled with a fifth order approximation to the Stokes theory of waves [9], with parameters given in Table 3 in terms of wave height H, period T and inverse of the steepness ratio S=H/λ.

The propagation of a sustained wave for several periods would require a larger domain, with extended forced and damped inlet and outlet regions [10]. The size of the total domain was reduced to limit the computational time with the aim of capturing the flow field around the structure.

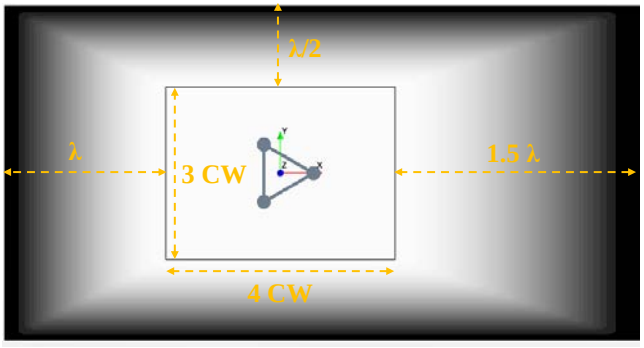

Figure 2. Top view of the wave forcing coefficient, with a rectangle showing the inner domain.

Table 3. Wave parameters (full-scale).

Test number	Wave height H (m)	Wave period T (s)	1/Steep. λ/H
2040	3.33	8	30
2050	6.30	11	30

2.1.2. Mooring. The mooring lines used for 6 DOF free motion simulations were modelled similar to the model test setup [2] through a spring-damper coupling of three horizontal lines connecting the top of each column with three anchors at the side of the wave tank. Each line is defined through a relaxation length, where no spring force is exerted, and a constant elastic coefficient. The damping coefficient is set to zero, so that the mooring system is modelled as a linear spring.

2.1.3. Mesh. A flexible approach was chosen for the mesh strategy, taking into account all different types of simulation, including the presence of the structure, waves and current. Refinement blocks were created in proximity of the structure and in areas of the domain with relevant flow features, such as the free surface and the wake downstream the columns.

The obtained mesh discretization is depicted in Figure 3 on the free surface and on the vertical centre plane showing the refinement blocks around the structure and the water-air interface.

A prismatic layer was generated around the columns and the pontoons to capture the boundary layer on the structure's walls. The near-wall layer has a height of 0.1 mm with the aim to achieve a y^+ value of 1, where a DES turbulent model with near wall treatment could be used. A total of 10 layers were built with a stretching ratio of 1.2.

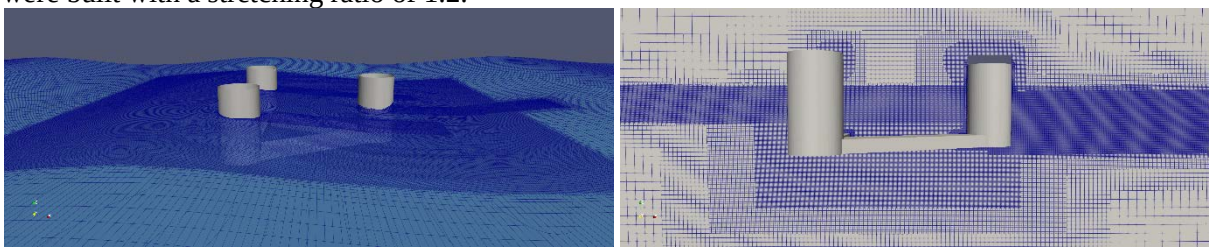

Figure 3. View of the mesh on the free surface (left) and on the vertical centre plane (right) showing the refinement blocks around the structure and water-air interface.

3. Results and discussion

Three different approaches for the platform motion were used; fixed (Sec. 3.1), i.e., restrained from motion, prescribed (Sec. 3.2), i.e., forcing the floater to follow the motion recorded during model tests and 6 DOF (Sec. 3.3), i.e., allowing the floater to move according to external forces from waves and mooring lines. Two different waves were analysed with full-scale parameters given in Table 3.

3.1. Restrained structure

Wave simulations are carried out with the platform restrained from motion and the wave pattern initialized in the whole domain with initial wave crest at the platform centre.

The surge force on the port and tower column are shown in Figure 4 for the last six periods and the corresponding mean value as dashed horizontal lines. A linear behaviour is observed for the lower sea state 2040, whereas higher harmonics characterize the higher sea state 2050.

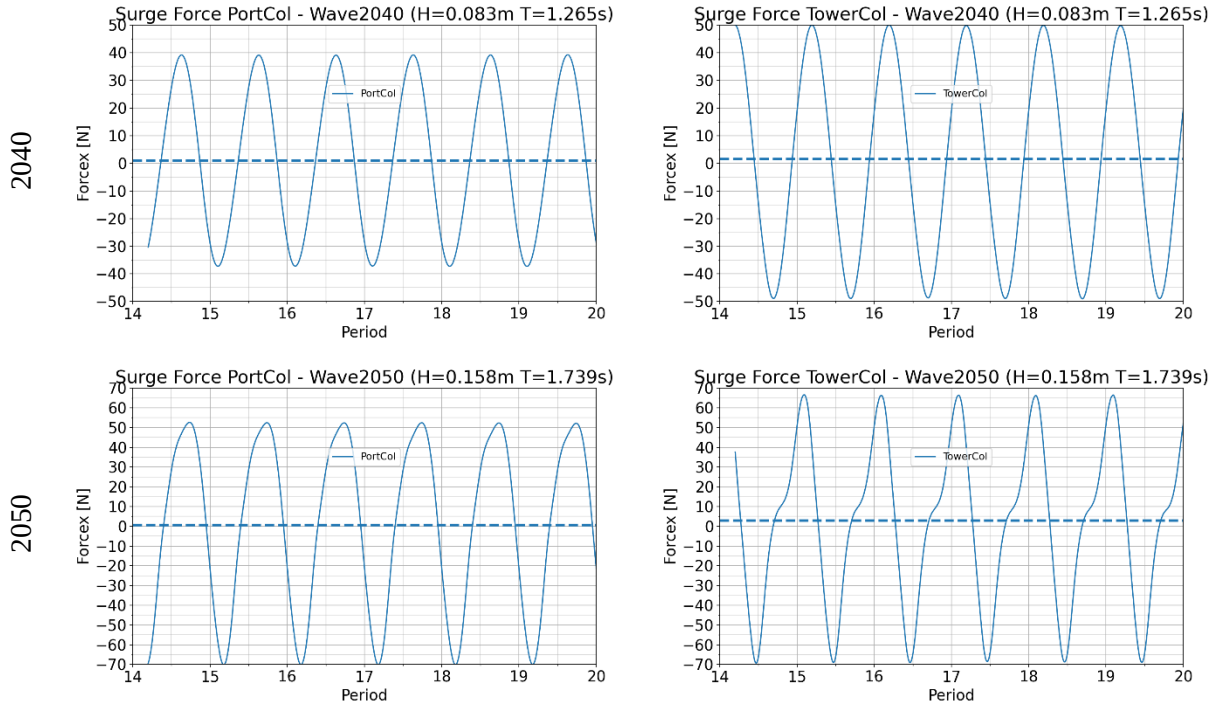

Figure 4. Surge force on the port (left) and tower (right) column for tests 2040 and 2050; dashed line shows the value averaged among the last 6 periods.

The corresponding sectional surge force is depicted in Figure 5 for the last two periods, only at the non-linear sea state 2050. The absolute value of the peak force has a minimum at the bottom of the column and increases almost linearly until reaching the section z_0 piercing the free surface, where it undergoes both a drop and a phase shift of the peak value. Sections not fully wetted by the incoming wave present a delayed increase of the force, visible in the zero up-crossing time instant. Drop of the force occurs however at the same instant for all sections, including those being partly wetted.

Differences can be observed between the upstream port column and the downstream tower column, which will be subject to the wake behind the upstream structure, including the port and starboard columns and the pontoons connecting the columns. The sectional force at the mean water level z_0 shows a larger peak value at the tower downstream column. The presence of higher order harmonics of the resulting loads is clearly visible for the higher sea state. While the average force remains close to zero for both sea states on the upstream column, an increase of the force with the sea state can be observed on the downstream tower column.

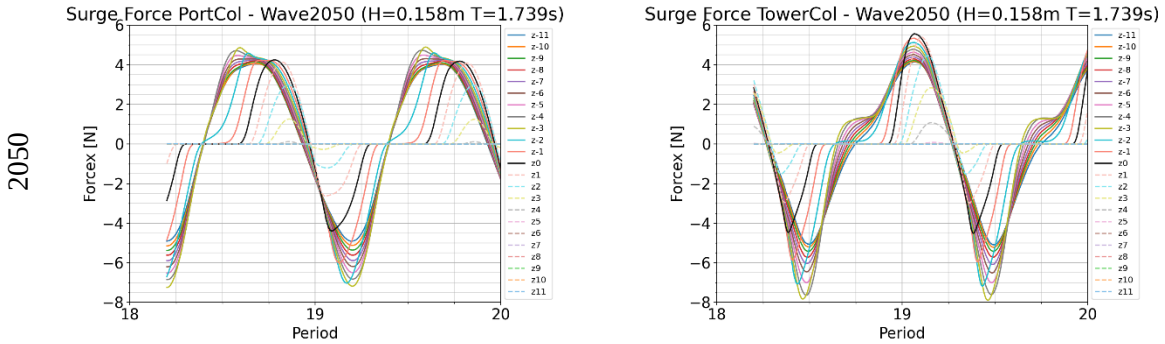

Figure 5. Sectional surge force on the port (left) and tower (right) column for test 2050.

3.2. Forced motion

Additional simulations were carried out forcing the platform to follow the motion obtained during model tests in regular waves [2]. Displacements and rotations of the platform's centre of mass recorded during experiments were used in CFD simulations to force the structure in all 6 degrees of freedom. Numerical simulations were synchronized with model tests by ensuring that the wave crest was located at the origin when starting the simulation.

The imposed motion allows the structure to follow the incoming wave. This can be observed in the surge force computed for the whole platform, whose amplitude is reduced of about one third for the motion case, compared to the restrained case (Figure 6). The same figure shows that the average surge force is also decreased for the setup with motion. Loads from forced motion simulations display a high-frequency noise, particularly for the test 2040. This noise follows the noise existing in the motion test data used as input for the numerical simulations.

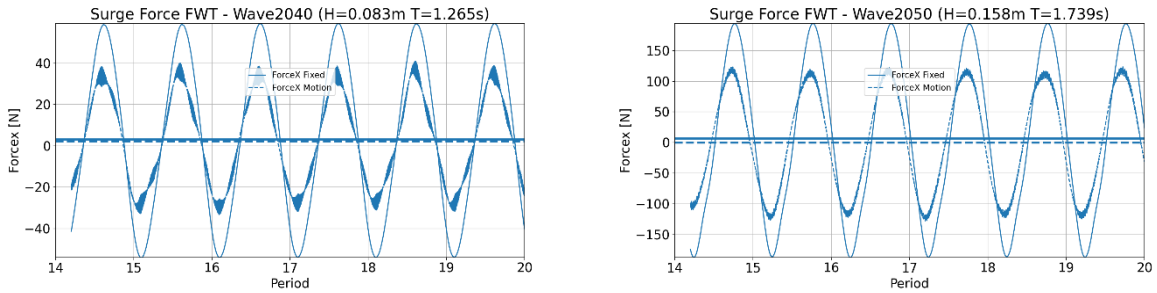

Figure 6. Comparison of the surge force on the platform between fixed (solid lines) and forced motion (dashed lines) for tests 2040 and 2050; horizontal lines show the value averaged among the last 6 periods.

A comparison of the surge force between fixed and forced motion is performed also on the single columns (Figure 7). The surge force on the upstream port column follows the trend of the whole platform, where load's amplitude and average values are reduced for the motion case, compared to the restrained case. Differences between the two motion approaches are smaller for the downstream tower column; for this column results obtained with forced motion are in general more regular, especially for the larger sea state. The corresponding sectional surge forces are shown in Figure 8, and follow the same trend observed for the global forces.

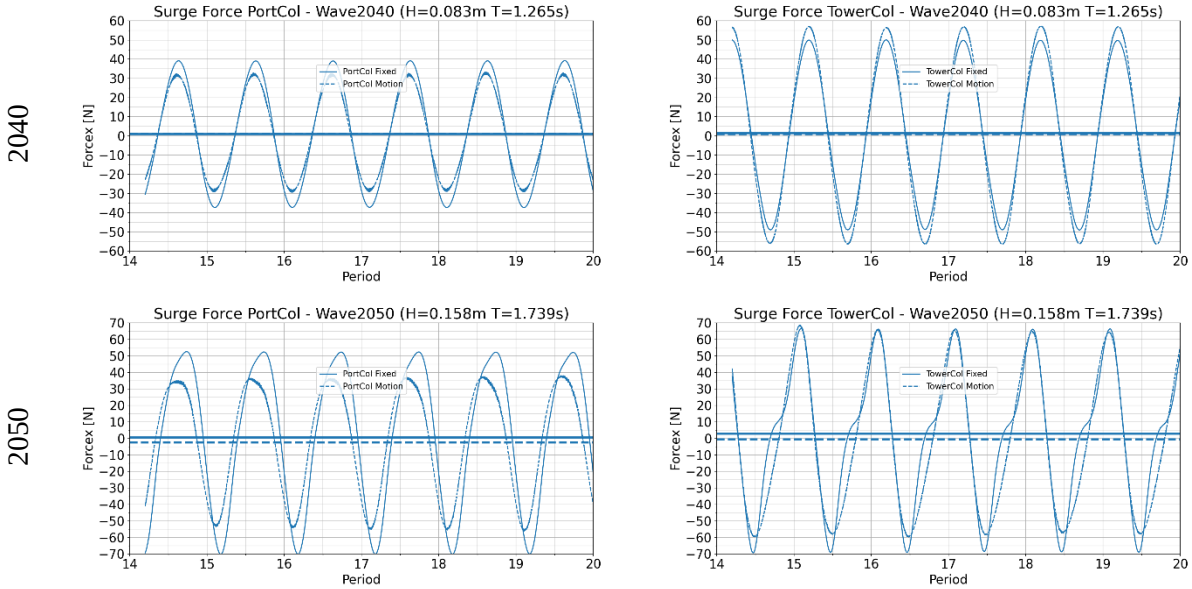

Figure 7. Comparison of the surge force on the port (left) and tower (right) column between fixed (solid lines) and forced motion (dashed lines) for tests 2040 and 2050; horizontal lines show the value averaged among the last 6 periods.

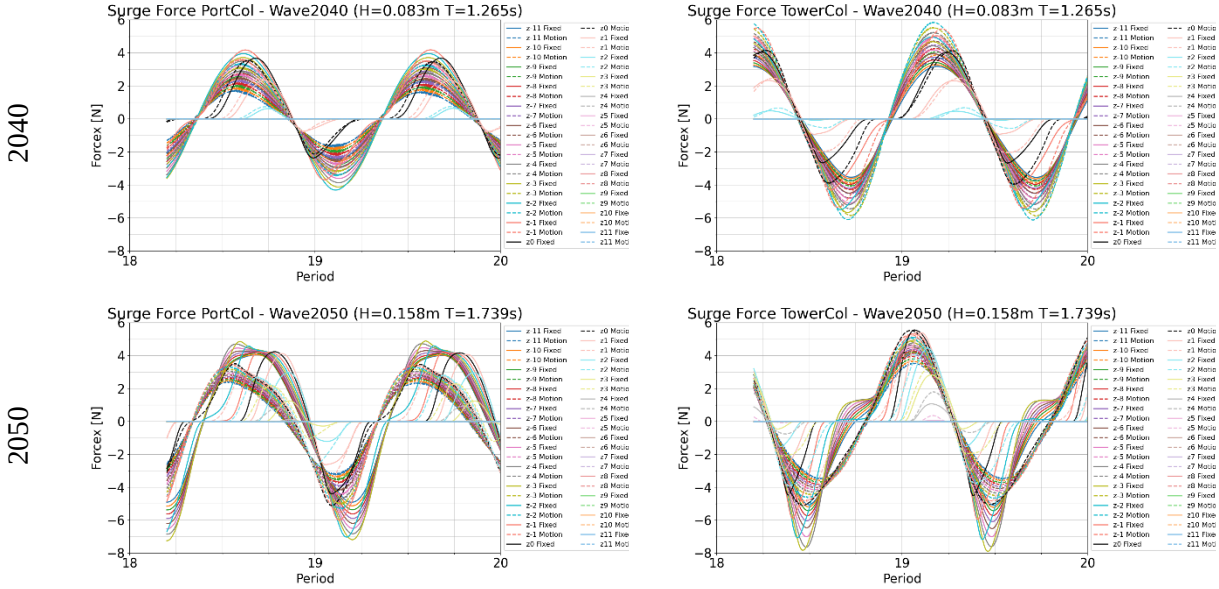

Figure 8. Comparison of the surge force on the port (left) and tower (right) column between fixed (solid lines) and forced motion (dashed lines) for tests 2040 and 2050.

3.3. Free motion

In order to study the six degrees of freedom free motion of the platform, the horizontal mooring lines used during model tests were modelled and simulations run in the same regular waves used for restrained and forced motion.

Results from these simulations are presented in Section 3.3.3. as comparison between forced "motion" and free "6DOF" motion.

3.3.1. Decay tests. The performance of the numerical moored model was initially assessed by means of decay tests in surge, heave and pitch. These tests are performed by imposing an offset in a single degree of freedom and let the structure oscillate back to its initial equilibrium position. A comparison of the obtained numerical results with the experiments is depicted in Figure 9 and tabulated in Table 4.

The decay periods obtained with CFD compare well with experiments for all three directions. After few oscillations the deviation become more pronounced. It can be observed that the initial offset used for the numerical simulations is slightly different from the one used in model tests, but this difference is deemed as negligible for the assessment of the natural period.

Table 4. Comparison of the natural periods between experiments and CFD (full-scale).

Mode	**Test [s]**	**CFD [s]**
Surge	93.7	96.6
Heave	16.4	17.4
Pitch	30.3	29.3

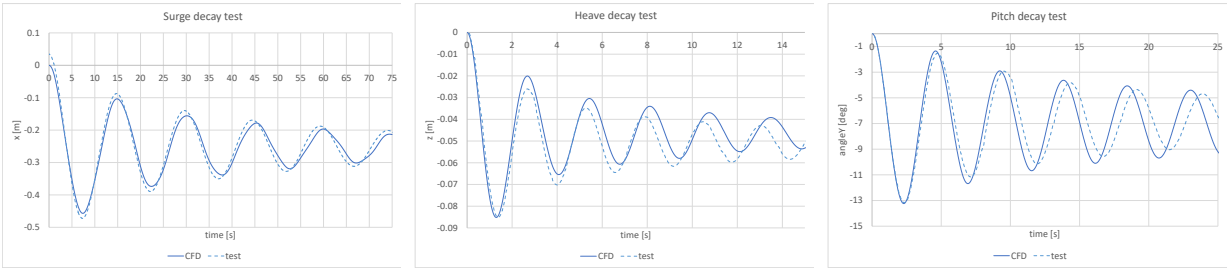

Figure 9. Comparison of the rigid motion between CFD and model tests for the decay tests in surge (left), heave (centre) and pitch (right).

3.3.2. Rigid motion. A comparison of the motion responses of the platform for surge and heave for tests 2040 and 2050 between CFD and experiments are presented in Figure 10 and Figure 11. Note that an offset of 0.05 m was added to the numerical heave motion as a constant deviation was observed with the experiments. There is a fair agreement in the displacement for all sea states.

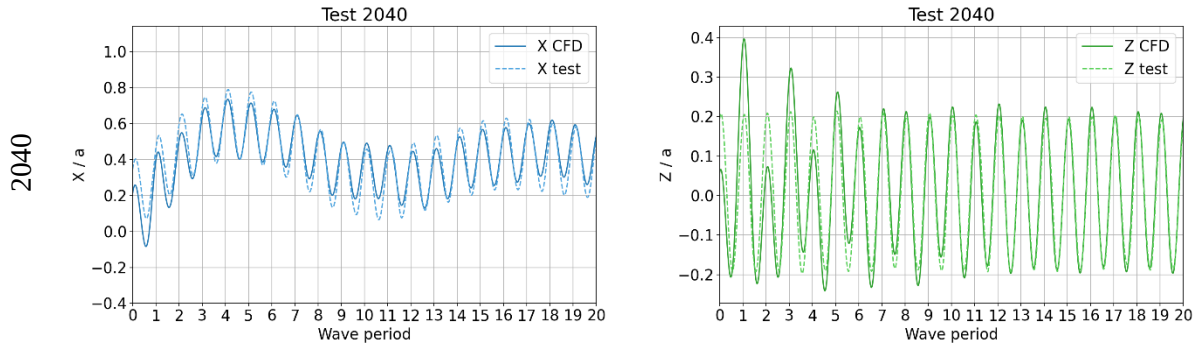

Figure 10. Comparison of the surge (left) and heave (right) rigid motion at the origin between CFD and experiments for test 2040.

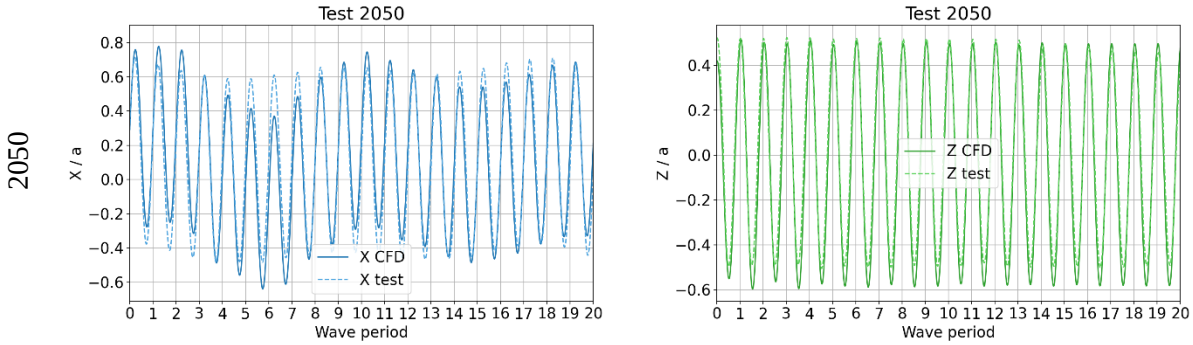

Figure 11. Comparison of the surge (left) and heave (right) rigid motion at the origin between CFD and experiments for test 2050.

3.3.3. Surge forces. 6 DOF free motion simulations were run to assess the capabilities to accurate predict the free rigid body motion of the platform subject to wave loads while constrained by mooring lines. A comparison of the surge force between forced "motion" and free "6DOF" motion is presented for the port and tower columns for tests 2040 and 2050 (Figure 12). The corresponding sectional loads are displayed in Figure 13. Not displayed in this article, loads on the whole platform computed with the two methods are overlapped.

The comparison shows a fair agreement between the two motion approaches, both in terms of global and local forces. The differences observed in the global forces for test 2050 in Figure 12 can be better understood through the local sectional forces in Figure 13, where differences in the force at the section located at the water level can be observed. Differences in the surge and heave motions would lead to different wet areas on the platform and therefore different loads.

Simulations with 6 DOF body motion are very demanding in terms of computational time and with the aim to assess local loads and flow features, a combination of model tests and numerical simulations with a forced motion approach would allow an accurate prediction of local flow features within a reduced computational time.

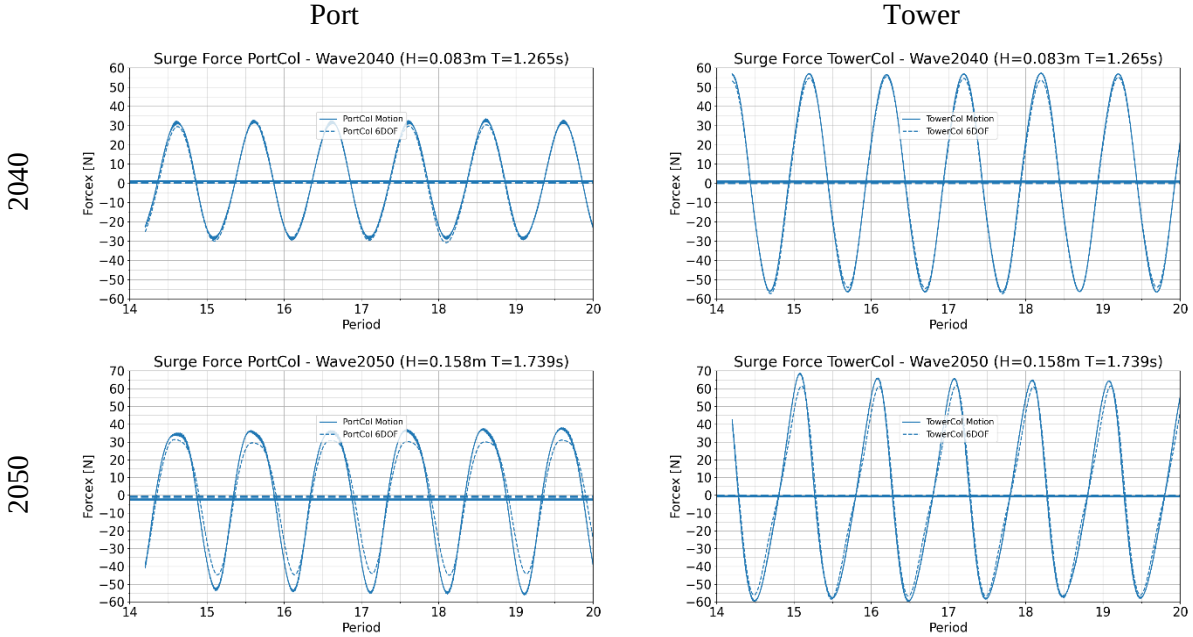

Figure 12. Comparison of the surge force on the port (left) and tower (right) column between forced (solid lines) and 6 DOF motion (dashed lines) for tests 2040 and 2050; horizontal lines show the value averaged among the last 6 periods.

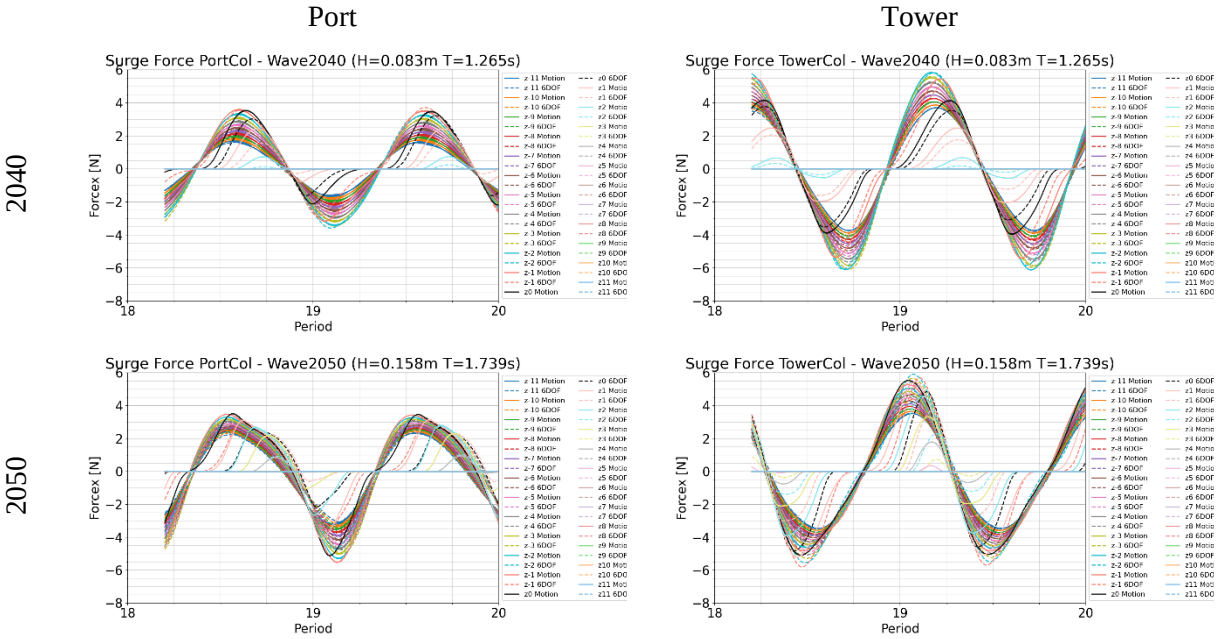

Figure 13. Comparison of the sectional surge force on the port (left) and tower (right) column between forced (solid lines) and 6 DOF motion (dashed lines) for tests 2040 and 2050.

4. Concluding remarks

CFD simulations were carried out on the 1:40 scale model of the INO WINDMOOR floater in regular waves to extract hydrodynamic loads, both on the structure, the single columns and sections from each column. Three different approaches for the platform motion were used, (i) fixed, i.e., restrained from motion, (ii) prescribed, i.e., forcing the floater to follow the motion recorded during model tests and (iii) 6 DOF, i.e., free to move according to external forces from waves and anchor lines.

The obtained results show the effect of the free surface on the local forces at sections with different submergences, especially around the water level. Sectional forces are also affected by the presence of the bottom pontoons. The tower column located in the wake behind the upstream columns and pontoons are subject to a more complex dynamic three dimensional flow, which is more difficult to predict through simplified methods based on the Morison equation and force coefficients.

A comparison of the surge force on the platform shows that the amplitudes of the loads obtained with motion are reduced compared to the corresponding fixed case. Results obtained with the moving platform are in general more regular, especially for larger sea states. The corresponding sectional surge forces follow the same trend observed for the global forces. The mean total surge force computed on the single columns and the whole platform show small quantitative differences between the different methods.

The motion responses of the platform for surge and heave obtained with CFD are in fair agreement with the experiments. Comparison to model tests would require a more systematic assessment of the wave kinematics between CFD and experiments, which has not been part of the present study.

Simulations with 6 DOF body motion are very demanding in terms of computational time and with the aim to assess local loads and flow features, a combination of model tests and numerical simulations with a forced motion approach would allow an accurate prediction of local flow features within a reduced computational time.

Acknowledgement

The research leading to these results has received funding from the Research Council of Norway through the following projects:

- FME NorthWind funded by the Research Council of Norway and industrial partners. This programme has funded research activities on 6 DOF platform motion waves;

- The WINDMOOR project funded by the Research Council of Norway under the ENERGIX programme (grant no. 294573) and industrial partners Equinor, MacGregor, Inocean, APL Norway and RWE Renewables. This project has funded research activities on fixed platform in waves;

- "High Resolution Numerical Modelling of Flexible Fish Cage Structures" project funded by the Research Council of Norway under the HAVBRUK2 programme (grant no. 267981). This project has funded research activities on forced platform motion in waves.

The author is grateful for the permission to use the INO WINDMOOR semisubmersible, which is jointly designed by Inocean and Equinor.

References

[1] C. E. Silva de Souza, P. A. Berthelsen, L. Eliassen, E. E. Bachynski, E. Engebretsen, and H. Haslum, ‘Definition of the INO WINDMOOR 12 MW base case floating wind turbine’, SINTEF Ocean, OC2020 A-044, Jan. 2021.

[2] M. Thys, C. E. Souza, T. Sauder, N. Fonseca, P. Berthelsen, E. Engebretsen, and H. Haslum, ‘Experimental Investigation of the Coupling Between Aero- and Hydrodynamical Loads on A 12 MW Semi-Submersible Floating Wind Turbine’, in *Proceedings of the International Conference on Offshore Mechanics and Arctic Engineering - OMAE,* Jun. 2021. doi: 10.1115/OMAE2021-62980.

[3] F. H. Dadmarzi, A. Califano, N. Fonseca, and P. A. Berthelsen, ‘Comparison of Morison Forces with CFD Modelling for a Surface Piercing Column of a FOWT’, in *Proceedings of the ASME 2022 International Offshore Wind Technical Conference*, Dec. 2022.

[4] P. A. Berthelsen, M. Thys, A. Kamath, T. Martin, and H. Bihs, ‘Numerical simulation and comparison with experiments of a floating wind turbine using a direct forcing method’, in *Proceedings of the 5th International Conference on Renewable Energies Offshore*, Lisbon, Portugal, Nov. 2022.

[5] Y. Wang and H.-C. Chen, ‘Verification and Validation of CFD Simulations of a FOWT Semi-submersible under Bichromatic and Random Waves’, *J. Offshore Mech. Arct. Eng.*, pp. 1–23, Dec. 2022, doi: 10.1115/1.4056421.

[6] L. Wang, A. Robertson, J. Kim, H. Jang, Z.-R. Shen, A. Koop, T. Bunnik, and K. Yu, ‘Validation of CFD simulations of the moored DeepCwind offshore wind semisubmersible in irregular waves’, *Ocean Eng.*, vol. 260, p. 112028, Sep. 2022, doi: 10.1016/j.oceaneng.2022.112028.

[7] J. Kim, J. O’Sullivan, and A. Read, ‘Ringing Analysis of a Vertical Cylinder by Euler Overlay Method’, presented at the ASME 2012 31st International Conference on Ocean, Offshore and Arctic Engineering, Rio de Janeiro, Jul. 2012.

[8] Siemens Digital Industries Software, ‘STAR-CCM+ version 2020.3 Build 15.06.007’. 2020.

[9] Fenton John D., ‘A Fifth-Order Stokes Theory for Steady Waves’, *J. Waterw. Port Coast. Ocean Eng.*, vol. 111, no. 2, pp. 216–234, Mar. 1985, doi: 10.1061/(ASCE)0733-950X(1985)111:2(216).

[10] B. Bouscasse, A. Califano, Y. M. Choi, X. Haihua, J. W. Kim, Y. J. Kim, S. H. Lee, H.-J. Lim, D. M. Park, M. Peric, Z. Shen, and S. M. Yeon, ‘Qualification Criteria and the Verification of Numerical Waves: Part 2: CFD-Based Numerical Wave Tank’, in *OMAE2021*, Volume 1: Offshore Technology, Jun. 2021. doi: 10.1115/OMAE2021-63710.